The experimental and theoretical QTAIMC study of the atomic and molecular interactions in dinitrogen tetroxide

Vladimir G. Tsirelson,[a]* **Anastasia V. Shishkina,**[a] **Adam I. Stash**[a,b] **and Simon Parsons**[c]

[a]Mendeleev University of Chemical Technology, Moscow 125047, Russia, [b]Karpov Institute of Physical Chemistry, Moscow 103064, Russia, and [c]School of Chemistry, The University of Edinburgh, Edinburgh EH9 3JJ, Scotland

Correspondence e-mail: tsirel@muctr.edu.ru

The atomic and molecular interactions in a crystal of dinitrogen tetraoxide, α-N_2O_4, have been studied in terms of the quantum topological theory of molecular structure using high-resolution, low-temperature X-ray diffraction data. The experimental electron density and electrostatic potential have been reconstructed with the Hansen–Coppens multipole model. In addition, the three-dimensional periodic electron density of crystalline α-N_2O_4 has been calculated at the B3LYP/cc-pVDZ level of theory with and without the geometry optimization. The application of the quantum theory of atoms in molecules and crystals (QTAIMC) recovered the two types of intermolecular bond paths between O atoms in crystalline α-N_2O_4, one measuring 3.094, the other 3.116 Å. The three-dimensional distribution of the Laplacian of the electron density around the O atoms showed that the lumps in the negative Laplacian fit the holes on the O atoms in the adjacent molecules, both atoms being linked by the intermolecular bond paths. This shows that the Lewis-type molecular complementarity contributes significantly to intermolecular bonding in crystalline N_2O_4. Partial overlap of atomic-like basins created by zero-flux surfaces in both the electron density and the electrostatic potential show that attractive electrostatic interaction exists between O atoms even though they carry the same net formal charge. The exchange and correlation contributions to the potential energy density were also computed by means of the model functionals, which use the experimental electron density and its derivatives. It was found that the intermolecular interactions in α-N_2O_4 are accompanied by the correlation energy-density 'bridges' lowering the local potential energy along the intermolecular $O\cdots O$ bond paths in the electron density, while the exchange energy density governs the shape of bounded molecules.

1. Introduction

Dinitrogen tetroxide, N_2O_4, is used extensively in organic synthesis, for example in nitration of aromatic compounds (Squadrito et al., 1990), nitrosation of amines (Boyer & Pillai, 1985), preparation of thionitrite (Oae et al., 1977) and sulfinyl nitrites (Oae et al., 1979), oxidation of olefins (Giamalva et al., 1987) and dethioacetalization reactions (Mehta & Uma, 1996). The high reactivity of N_2O_4 leads to the creation of complexes with organic, polymeric and inorganic compounds which are useful reagents in organic reactions, for example in the synthesis of organo-amino derivatives of C_{60} (Anantharaj et al., 1999). N_2O_4 is also used as the oxidant in rocket propellants.

647

Raman (Parts & Miller, 1965; Bolduan & Jodl, 1982; Bolduan *et al.*, 1984) and IR (Hisatsune *et al.*, 1960; Parts & Miller, 1965) spectroscopy of solid N_2O_4, the study of solid-state and thin-film autoionization processes (Bolduan *et al.*, 1984; Jones *et al.*, 1985), and B3LYP/6-311++G(3df) calculations (Zakharov *et al.*, 2008) point to the existence of six possible isomers of the N_2O_4 molecule. Gas-phase electron diffraction (McClelland *et al.*, 1972) and rotationally resolved IR spectroscopy (Domenech *et al.*, 1994) have shown that the most stable conformation of the molecule is the planar D_{2h} structure. This structure is sometimes considered to be a dimer, in which the NO_2 moieties are linked by a weak N—N bond (r_{N-N} = 1.75–1.78 Å compared with r_{N-N} = 1.45 Å in hydrazine).

The electronic structure and bonding for the ground state of the free N_2O_4 molecule were investigated using various levels of theory including CCSD(T) (Wesolowski *et al.*, 1997; Glendening & Halpern, 2007), B3LYP (Messerschmidt *et al.*, 2002), MC-CASSCF (Bauschlicher *et al.*, 1983), and multi-reference CASSCF/CASPT2 methods (Koput, 1995; Andersson & Roos, 1993). The CCSD(T) method with double-zeta and triple-zeta Huzinaga–Dunning basis sets yielded geometrical parameters which are the same as those obtained by rotationally resolved IR spectroscopy, *i.e.* the N—N distance was 1.756 Å (Domenech *et al.*, 1994). Molecular orbital consideration, electron-localization function and QTAIMC (Bader, 1990) calculations on the free molecule based on the B3LYP/cc-pvTZ wavefunction have all shown that the major contribution to the N—N bond arises from the σ-HOMO (Chesnut & Crumbliss, 2005).

Dinitrogen tetroxide crystallizes below 262 K (Giauque & Kemp, 1938) in two forms, which both contain planar symmetric O_2N-NO_2 molecules. The low-temperature cubic phase (α-N_2O_4, space group $Im\bar{3}$, Fig. 1) is obtained from the condensed gas, and neutron diffraction data show that this form is retained between 20 and 140 K (Kvick *et al.*, 1982). At high pressure, laser irradiation of α-N_2O_4 caused the formation of β-N_2O_4, which is also composed of planar N_2O_4 molecules. When the pressure is increased to 76 kbar, β-N_2O_4 undergoes a reversible phase transformation to the ionic, crystalline $NO^+NO_3^-$ form, while α-N_2O_4 is apparently stable (Angew *et al.*, 1983).

The experimental and theoretical charge densities in α-N_2O_4 were previously analyzed by Messerschmidt *et al.* (2002) using the QTAIMC approach. They concluded that the rather long N—N bond distance may be attributed to strong repulsion between the oxygen lone pairs and between the positively charged N atoms. The lone pairs of the O atoms were also shown to be involved in the π bonds. Valence atomic monopoles led to atomic charges O = +0.06 (1) and N = −0.12 (1) e, which apparently conflict with the relative electronegativities of O and N atoms, and it was notable that although they were found to be insensitive to the theoretical method used, QTAIMC atomic charges were consistently higher than the experimental ones.

Rather less is known about the nature of molecular interactions in crystalline α-N_2O_4, and it is this that forms the focus

of the present paper. In the absence of charge transfer or hydrogen bonding, non-polar molecular solids are held together by weak van der Waals (vdW) forces, which are mainly attributed to electron-correlation (dispersion) interactions (Chałasiński & Szczęśniak, 1994). In this paper we aim to describe the intermolecular van der Waals interactions in α-N_2O_4 qualitatively and quantitatively by applying the QTAIMC (Bader, 1990). Our study is based on a combination of experimental low-temperature X-ray diffraction data and quantum-chemical calculations. In order to analyse the role of electrostatic interactions we have performed a quantum-topological analysis of the electrostatic potential, a method which has recently become popular (Pathak & Gadre, 1990; Gadre *et al.*, 1996; Leboeuf *et al.*, 1997, 1999; Zhurova *et al.*, 2001, 2002; Tsirelson & Ozerov, 1996; Tsirelson *et al.*, 2000, 2001; Balanarayan & Gadre, 2003; Bouhmaida *et al.*, 2002; Mata *et al.*, 2007; Novakovic *et al.*, 2007). The exchange and correlation energy densities in α-N_2O_4 were also computed using functionals based on the experimental electron density and its derivatives (Tsirelson, 2007). Results from this analysis demonstrate that the 'bridges' of correlation energy density lower the local potential energy along the intermolecular $O\cdots O$ bond paths. We will also show that the exchange energy density determines the shape of molecules, favouring the bonding. Thus, our work develops the previous QTAIMC experimental and theoretical studies of the electron-density features in the van der Waals crystals Cl_2 (Tsirelson *et al.*, 1995), ClF (Boese *et al.*, 1997) and S_4N_4 (Scherer *et al.*, 2000).
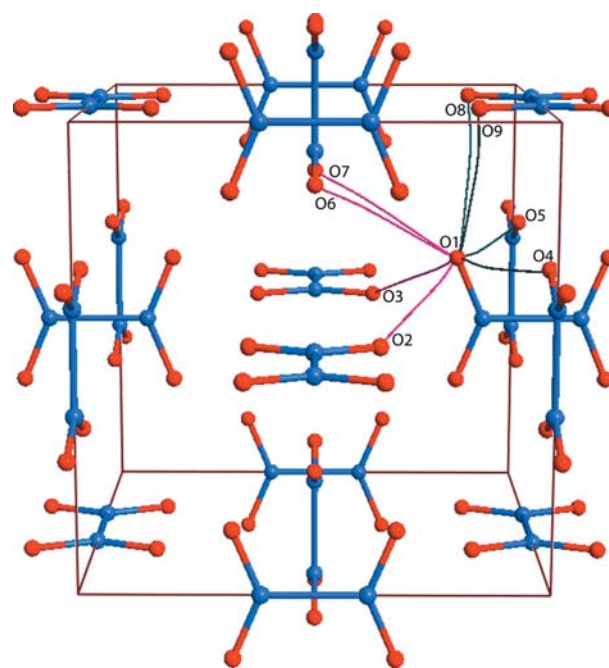

Figure 1
Unit cell of the N_2O_4 crystal with intermolecular bond paths of type I (3.116 Å, pink) and type II (3.094 Å, green).

Table 1
Crystallographic data, selected experimental information and the reliability factors for N_2O_4.

|	
Crystal data	
Chemical formula	N_2O_4
M_r	92.01
Crystal system, space group	Cubic, $Im\bar{3}$
Temperature (K)	100.0
a (Å)	7.7529 (1)
V (Å^3)	466.01 (1)
Z	6
Radiation type	Mo $K\alpha$
Wavelength (Å)	0.71073
μ (mm^{-1})	0.22
Crystal form, size (mm)	Cylinder, $0.4 \times 0.4 \times 1.0$
Data collection	
Diffractometer	Area
Data-collection method	ω scans
Absorption correction	Multi-scan†
T_{min}, T_{max}	0.72, 0.92
Number of measured, independent and observed [$I>2\sigma(I)$] reflections	11 365, 516, 476
R_{int}	0.025
θ_{max} (°)	52.3
$(\sin\theta/\lambda)_{max}$ (Å^{-1})	1.11
Refinement	
Refinement on	F^2
Spherical-atom model, harmonic approximation for atomic displacements (11 parameters)	$R = 0.0278$, $wR = 0.0752$, $S = 1.03$
Weighting scheme, w‡ (spherical-atom model)	$a = 0.05$, $b = 0.04$, $c = 0.0$
Multipole model, harmonic approximation for atomic displacements (31 parameters)	$R = 0.0151$, $wR = 0.0231$, $S = 1.44$
Weighting scheme, $w*$‡ (multipole model)	$a = 0.05$, $b = 0.05$, $c = 4.5$
No. of reflections	508
No. of parameters	11
$(\Delta/\sigma)_{max}$	0.001
$\Delta\rho_{max}$, $\Delta\rho_{min}$ (e Å^{-3})	0.26, −0.21

† Based on symmetry-related measurements. ‡ $w = \exp[c(\sin\theta/\lambda)^2]/\sigma^2(F_o^2) + (ap)^2 + bp$, where $p = (F_o^2 + 2F_c^2)/3$ (Sheldrick, 2008).

2. Experimental

A crystal of α-N_2O_4 was grown using a laser-assisted zone-refinement method (Boese & Nussbaumer, 1994) at 253 K in a capillary (o.d. 0.4 mm) mounted on a Bruker Smart Apex diffractometer equipped with a SMART APEX CCD detector and an Oxford Cryosystems cooling device. The crystal was cooled to 100 K and intensities of 11 365 reflections were collected with 2θ set at −20, −40 and −75° in steps of 0.2° (ω scans, $2\theta < 105°$). The data integration and unit-cell refinement were performed with the program *SAINT* (Siemens, 1996). The intensities were reduced to a common scale and averaged using the program *SORTAV* (Blessing, 1987, 1989); 516 independent reflections ($R_{int} = 0.025$) were finally obtained.

The structure of N_2O_4 was solved by direct methods (*SHELXS*; Sheldrick, 2008) and refined by full-matrix least-squares against F^2 in the anisotropic approximation for atomic displacement using *CRYSTALS* (Betteridge *et al.*, 2003). The subsequent multipole refinement ($l \leq 3$) was carried out within the Hansen–Coppens (Hansen & Coppens, 1978)

formalism using the modified *MOLDOS*97 program (Protas, 1997). The relativistic wavefunctions by Macchi & Coppens (2001) were used to describe the core and valence electron density. The refinement was carried out against F using 476 reflections with $I > 2\sigma(I)$, converging to $R = 0.0151$, $wR = 0.0231$, goodness-of-fit $S = 1.44$ (for weighting scheme see Table 1). These data compare with $R(F) = 0.021$, $wR = 0.053$, $S = 1.45$ obtained by Messerschmidt *et al.* (2002). Positional
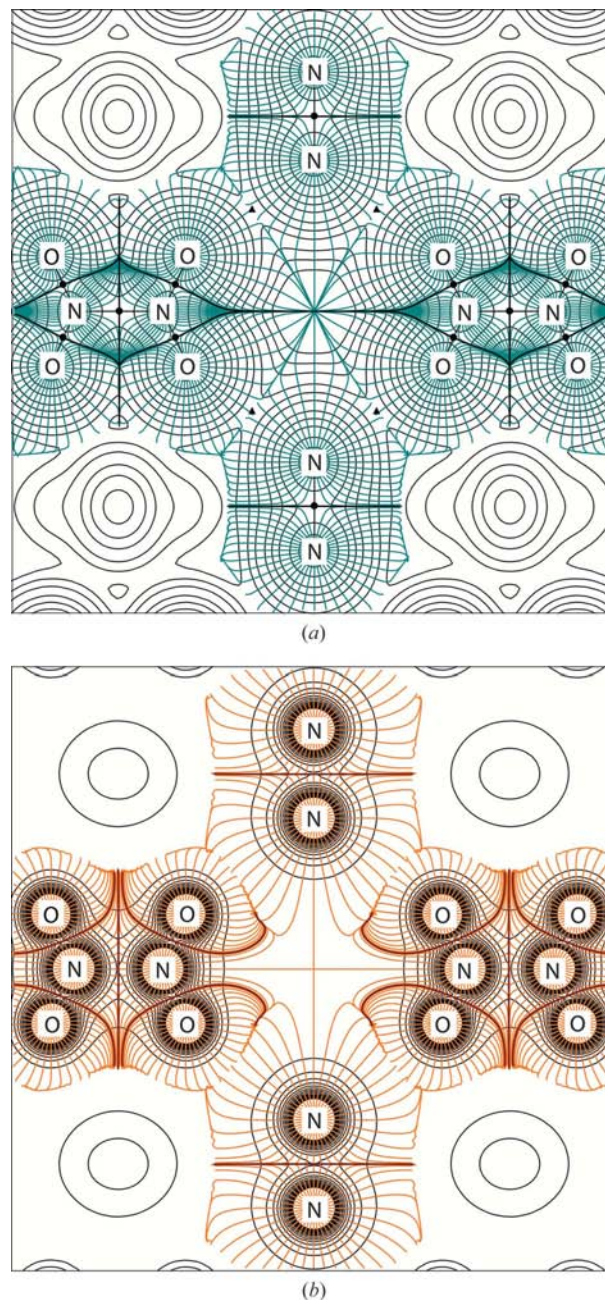
Figure 2
The gradient fields of (*a*) the experimental electron density and (*b*) the experimental electrostatic potential superimposed on the experimental electron density and electrostatic potential; the (100) plane of the unit cell is shown. The bold lines correspond to the zero-flux atomic boundaries. The critical points (3, −1) and (3, +1) in electron density are marked by black rings and triangles.
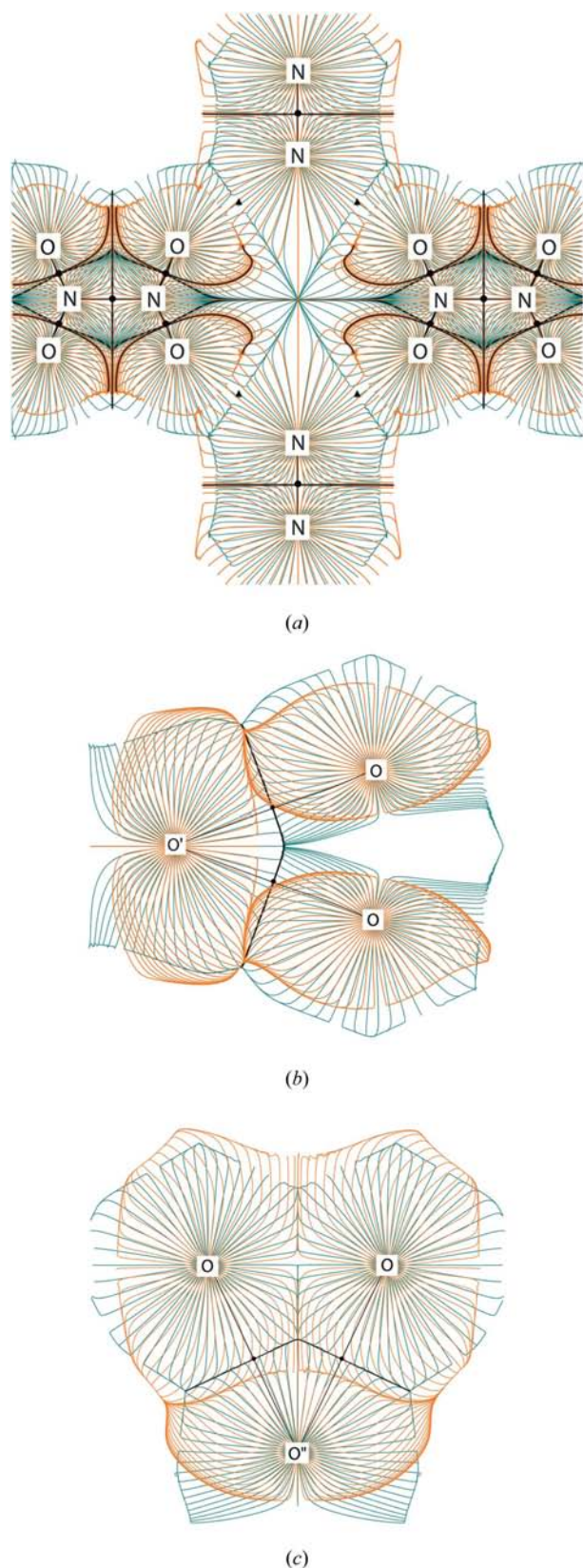
(a)

(b)

(c)

Figure 3
The superposition of gradient fields in the experimental electron density (green) and electrostatic potential (orange): (*a*) the (100) plane of the unit cell; (*b*) the plane containing intermolecular O···O bond paths of type I; (*c*) the plane containing intermolecular O···O bond paths of type II. The bold lines correspond to the zero-flux atomic boundaries.

and anisotropic harmonic atomic displacement parameters were refined using high-angle (sin $\theta/\lambda > 0.7$ Å) reflections, while the multipole parameters were refined using the total data set. The Becker & Coppens (1974) isotropic secondary extinction proved to be negligible in our sample.

The validity of the refinement was checked using an Abrahams–Keve (Abrahams & Keve, 1971) plot. It was also found that bonded pairs of atoms satisfy the Hirshfeld (1976) rigid-bond criteria, according to which the difference in atomic vibration amplitudes of two bonded atoms in the direction of the bond between them must be $\sim 10^{-4}$ Å^2. We obtained z^2(N—O) = 1.9×10^{-4} Å^2, z^2(N—N) = 0 Å^2 (by symmetry).

The residual multipole-model electron density varies from -0.13 to 0.17 e Å^{-3}. The error in the experimental electron density was estimated according to Lobanov *et al.* (1990). The electron-density error at the middle of the N—N and N—O distances is 0.003 and 0.015 e Å^{-3}. Between O atoms bonded by the van der Waals interactions, this error is ~ 0.001 e Å^{-3}.

Crystallographic data and selected experimental information as well as the reliability factors are given in Table 1. The structure factors, atomic coordinates, displacement and multipole parameters as well as the residual electron-density maps and the interatomic electron-density error distributions have been deposited.[1]

The multipole parameters were used to calculate the quasi-static electron density (ED) and deformation ED (see supplementary materials). The QTAIMC analysis was then performed, yielding the maps of gradient fields of the experimental electron density and electrostatic potential shown in Figs. 2 and 3. The Laplacians of experimental and theoretical ED were also calculated (Figs. 4–6). The features of the bond-critical points in the ED were estimated, including kinetic, potential and total electronic energy densities, $g_b(\mathbf{r})$, $v_b(\mathbf{r})$, and $h_b(\mathbf{r})$ (Table 2). The latter were computed using a combination of the local virial theorem (Bader & Beddall, 1972) and Kirzhnits' (1957) formula for kinetic electronic energy density, $g_b(\mathbf{r})$ (Tsirelson & Stash, 2004). Also evaluated were the atomic volumes, the atomic electron populations integrated within zero-flux surfaces of the atomic basins, atomic charges and atomic electronic energies. These quantities are listed in Table 3. All the calculations were performed with the *WinXPRO* program (Stash & Tsirelson, 2002, 2005).

3. Computational

Calculations of a periodic infinite α-N$_2$O$_4$ crystal have been carried out by the Kohn–Sham method using the program *CRYSTAL*06 (Dovesi *et al.*, 2006). The level of accuracy in evaluating the Coulomb and exchange series was controlled using default values for the five standard threshold values included in *CRYSTAL*06. The density-functional theory (DFT) exchange-correlation contribution was evaluated by numerical integration over the unit cell (Pascale *et al.*, 2004).

---

[1] Supplementary data for this paper are available from the IUCr electronic archives (Reference: SO5026). Services for accessing these data are described at the back of the journal.

The (55, 434)p atomic grid generated through Gauss–Legendre and Lebedev quadrature schemes has been used. That grid contains 55 radial points and a variable number of angular points, with a maximum of 434 on the Lebedev surface in the most accurate integration region. The condition for the SCF convergence was set to 10^{-11} on the root-mean-square (r.m.s.) variation of the density-matrix elements between two subsequent cycles. The shrinking factor of the commensurate reciprocal-space grid was set to 8, corresponding to 35 k points in the irreducible Brillouin zone at which the Hamiltonian matrix was diagonalized. The total energies obtained with this mesh were fully converged.

The crystal structure optimization was performed by means of a quasi-Newton algorithm in which the quadratic step (Broyden–Fletcher–Goldfarb–Shanno Hessian updating

scheme) was combined with a linear one, as proposed by Schlegel (1982). Convergence was tested on the r.m.s. and the absolute value of the largest component of the gradients and the estimated displacements. The thresholds for the maximum force, the r.m.s. force, the maximum atomic displacement, and the r.m.s. atomic displacement on all atoms have been set to 0.00045, 0.00030, 0.00180 and 0.00120 a.u., respectively. The structure optimization was considered complete when the four conditions were simultaneously satisfied.

Starting from the experimental crystal structural parameters and fixing the crystal space group, a full optimization of both lattice parameters and atomic coordinates was carried out. To elucidate the basis-set effect on the calculated geometry three basis sets were used: Pople's basis-set family 6-31G* and 6-311G* and the correlation-consistent cc-pVDZ basis sets by Dunning & Woon (1995). The BLYP (Becke, 1988a; Lee et al., 1988), PWGGA (Perdew, 1991), PBE (Perdew et al., 1996) and B3LYP (Becke, 1993; Lee et al., 1988; Miehlich et al., 1989) exchange-correlation functionals were all tested. The absence of imaginary frequencies was observed for all the methods mentioned above. The unit-cell parameters obtained in these calculations are listed in Table 4. Although the BLYP/6-31G* approximation provided the lowest energy value, the B3LYP/cc-pVDZ method gave the unit-cell parameter $a = 7.780$ Å, which was the closest to the experimental value ($a = 7.7546$ Å). Therefore, we used the results of the B3LYP/cc-pVDZ calculation (calculation 1) for the subsequent investigation of intra- and intermolecular interactions in this crystal.

We also tested another version of the B3LYP/cc-pVDZ calculation (hereafter calculation 2) in which the cell parameters of the crystal were fixed to the experimental values, while the atomic coordinates were optimized. A comparison of this simplified calculation with calculation 1 will be described below.

Theoretical structure factors were computed from calculation 1, and the same refinement of the Hansen–Coppen's (Hansen & Coppens, 1978) static multipole model (model/CRYSTAL) as
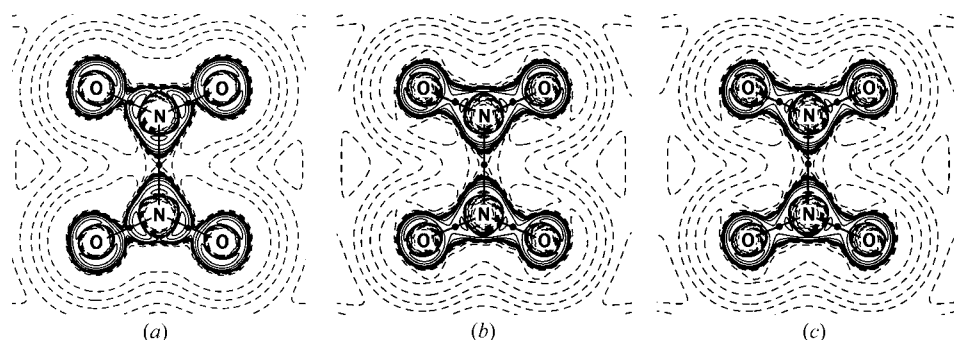

Figure 4
The Laplacian of electron density in the (100) plane of the unit cell: (a) model electron density derived from the X-ray diffraction experiment; (b) B3LYP/cc-pvDZ/CRYSTAL calculation (1); (c) B3LYP/cc-pvDZ/CRYSTAL calculation (2) – see text for explanations. Solid and broken lines represent negative and positive Laplacian values. Line intervals are $\pm 2 \times 10^n$, $\pm 4 \times 10^n$ and $\pm 8 \times 10^n$ e Å^{-5} ($-2 \le n \le 2$).

Figure 5
The Laplacian of electron density in N_2O_4 in planes containing intermolecular O$\cdots$O bond paths of type II (top) and type I (bottom). Solid and broken lines represent negative and positive Laplacian values. Line intervals are $\pm 2 \times 10^n$, $\pm 4 \times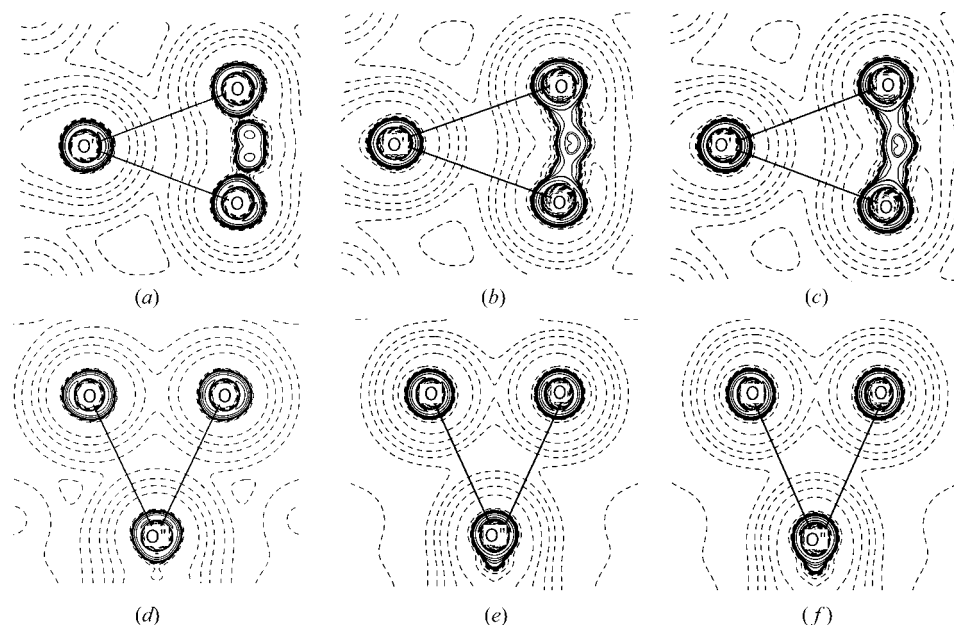 10^n$ and $\pm 8 \times 10^n$ e Å^{-5} ($-2 \le n \le 2$); (a, d) experiment; (b, e) B3LYP/cc-pvDZ/CRYSTAL (1); (c, f) B3LYP/cc-pvDZ/ CRYSTAL (2).

Vladimir G. Tsirelson et al. · Study of atomic and molecular interactions

that used for experimental data was performed. The same reflections were used in the refinement yielding $R = 0.0057$, $wR = 0.0054$ and $S = 0.89$. A unit weighting scheme was applied for the uniformly precise theoretical structure factors. As a result, we obtained a theoretical model electron density in the same form as the experimental one, and quantum-topological analysis of these data was performed in the same way as described above for the experimental data. Comparisons are available in Table 2 and Figs 4 and 5.

4. Results and discussion

4.1. Atomic characteristics and intramolecular interactions: electron-density analysis

Atomic electron populations in α-N_2O_4 were computed by integration of both experimental and theoretical electron
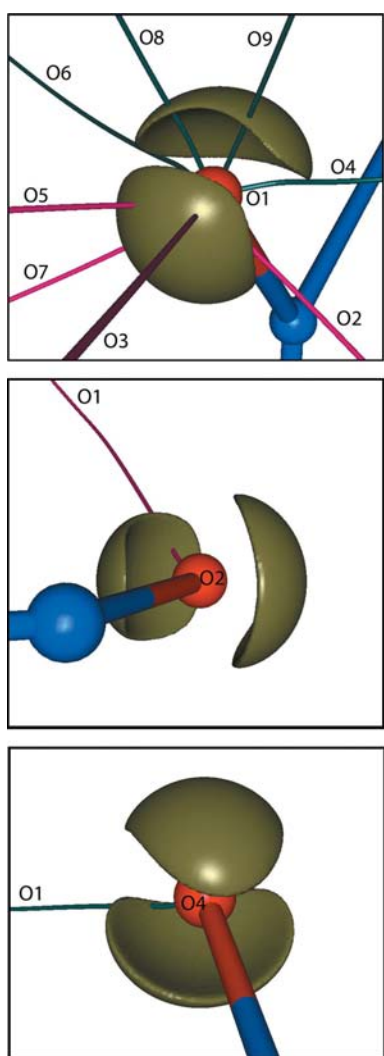

Figure 6
Three-dimensional isosurfaces of the Laplacian of valence electron density $\nabla^2 \rho(r) = -85$ e Å^{-5} (the 'lumps') together with the bond paths for fragments of the N_2O_4 crystal illustrating the intermolecular O$\cdots$O interactions.

densities within the atomic basins restricted by zero-flux surfaces in the electron-density gradient field (ρ basins). The net atomic charges determined from these quantities are listed in Table 3. The experimental and theoretical QTAIMC atomic charges agree within 0.1 e. They also agree reasonably well with those of Messerschmidt et al. (2002) derived by QTAIMC from single-molecule calculations by Hartree–Fock, B3LYP and MP2 methods using the 6-31G(d), 6-31+G(d) and 6-311+G(3df) basis sets (N: +0.71 to +0.86 e; O: -0.36 to -0.43 e), as well as from the periodic HF/6-21G(d) and B3LYP/6-21G(d) calculations (N: +0.83 to +0.94 e; O: -0.41 to -0.47 e). At the same time, they differ noticeably from the experimental QTAIMC atomic charges by Messerschmidt et al. (2002): +0.46 e for N and -0.24 e for O. The possible reason for the discrepancy may be the deficiency of Messerschmidt et al.'s multipole model mentioned in §1: the valence atomic monopoles lead to atomic charges O = +0.06 (1) and N = -0.12 (1) e which conflict with the relative electronegativities of O and N. For comparison, our valence atomic monopoles are O = -0.05 (1) and N = + 0.10 (1) e. In addition, many of the multipole parameters in Messerschmidt et al. (2002) are small in value and comparable with their standard uncertainties (see supplementary materials).

The experimental electron-density gradient fields depicted in Figs. 2 and 3 show that atomic volumes in the crystalline N_2O_4 have strongly aspherical shapes. The volume of an O atom, $\Omega(O) = 16.140$ Å^3, is ca 2.45 times that of a N atom, $\Omega(N) = 6.561$ Å^3. Atomic volumes yield additive contributions to the molecular polarizability (Bader et al., 1992) and, therefore, we can conclude that O atoms mainly define the dispersion interaction of the N_2O_4 molecules.

The sum of zero-flux atomic volumes over the unit cell reproduces the X-ray experimental volume within 0.02% (Table 1). Similarly, the sum of atomic electronic energies yields the total 'experimental' electronic energy of the (bonded) molecule $E_{mol} = -409.290$ hartree. Comparing the electronic energy values derived from the wavefunctions for a molecule and a crystal in different ways (see Table 4), we can see that the spread of these quantities is $\sim 1\%$. This is consistent with early theoretical conclusions (Politzer & Parr, 1974; Tal & Bader, 1978; Reznik, 1992) based on Kirzhnits-expansion computations of the average molecular energies from the Hartree–Fock wavefunction. Unfortunately, the uncertainty of 1% is too large to allow determination of intermolecular interaction energies in crystalline α-N_2O_4. This conclusion is in agreement with other QTAIMC estimates of electronic energy in crystals (Tsirelson et al., 2006; Zhurova, Stash et al., 2006).

Inspection of Figs. 4 and 5, and Table 2 shows that calculation of the Laplacian distributions and bond-critical point (BCP) characteristics from the B3LYP/cc-pvDZ/CRYSTAL wavefunctions 1 and 2 lead to the same results. We shall use the results from wavefunction 1 in the following discussion.

The experimental and theoretical wavefunction-based Laplacian values at the BCPs are close to each other for the N—N bond, but their agreement for the N—O bond is worse (Table 2). The same applies to the general picture of the

Table 2
The characteristics of the bond-critical points in N_2O_4.

R is the bond length, $\rho_b(\mathbf{r})$ is the electron density, $\nabla^2\rho_b(\mathbf{r})$ is the Laplacian of electron density, $g_b(\mathbf{r})$, $v_b(\mathbf{r})$ and $h_b(\mathbf{r})$ are kinetic, potential and electronic energy densities. The first line presents the model electron-density data (experiment), the second line is the model electron-density data derived by multipole refinement using B3LYP/cc-pvDZ/CRYSTAL structure factors computed after total structure optimization, the third-line data calculated from the B3LYP/cc-pvDZ/CRYSTAL (1) wavefunction; full optimization of atomic coordinates and cell parameters have been performed; the fourth-line data calculated from the B3LYP/cc-pvDZ/CRYSTAL (2) wavefunction (atomic coordinates were optimized while cell parameters were fixed at the experimental values). Procrystal values are given in square brackets.

	R (Å)	$\rho_b(\mathbf{r})$ (a.u.)	$\nabla^2\rho_b(\mathbf{r})$, a.u.	$g_b(\mathbf{r})$ (a.u.)	$v_b(\mathbf{r})$ (a.u.)	$h_b(\mathbf{r})$ (a.u.)
N—N†	1.759 (1)	0.164 (4)‡	0.081 (2)	0.155	−0.290	−0.135
		[0.125]	[0.368]			
	1.774	0.149	0.123	0.140	−0.250	−0.110
	1.774	0.146	0.060	0.076	−0.137	−0.061
	1.773	0.147	0.059	0.076	−0.137	−0.061
N—O§	1.190 (1)	0.532 (4)	−0.536 (13)	0.914	−1.961	−1.048
		[0.467]	[0.181]			
	1.190	0.518	−0.619	0.855	−1.865	−1.010
	1.190	0.543	−1.225	0.460	−1.118	−0.658
	1.190	0.544	−1.226	0.460	−1.118	0.658
O···O′¶ (Type I)	3.116 (1)	0.004 (1)	0.022 (2)	0.004	−0.003	0.001
	3.127	0.004	0.022	0.004	−0.002	0.002
	3.127	0.005	0.022	0.005	−0.004	0.001
	3.110	0.005	0.023	0.005	−0.004	0.001
O···O″¶(Type II)	3.094 (1)	0.004 (1)	0.023 (2)	0.004	−0.003	0.001
		[0.005]	[0.024]			
	3.108	0.004	0.023	0.004	−0.003	0.001
	3.108	0.005	0.023	0.005	−0.004	0.001
	3.096	0.005	0.023	0.005	−0.004	0.001

† R(N—O): 1.1902 (3) Å (X-ray diffraction; Messerschmidt *et al.*, 2002); 1.196 Å [single molecule, B3LYP/6-31G(d); Messerschmidt *et al.*, 2002]; 1.190 (2) Å (electron diffraction at 252 K; McClelland *et al.*, 1972), 1.1855 (9) Å (neutron diffraction at 100 K; Kvick *et al.*, 1982), 1.196 (5) Å (rotationally resolved IR spectroscopy at 50 K; Domenech *et al.*, 1994). ‡ Values obtained by Messerschmidt *et al.* (2002) (atomic units) are: ρ_b (N—N) = 0.180 (1), $\nabla^2\rho_b$ (N—N) = 0.034 (1), ρ_b(N—O) = 0.544 (4); $\nabla^2\rho_b$ (N—O) = −1.133 (5). § R(N—N): 1.7586 (7) Å (X-ray diffraction; Messerschmidt *et al.*, 2002), 1.781 Å [single molecule, B3LYP/6-31G(d); Messerschmidt *et al.*, 2002], 1.782 (8) Å (electron diffraction at 252 K; McClelland *et al.*, 1972), 1.756 (1) Å (neutron diffraction at 100 K; Kvick *et al.*, 1982), 1.756 (10) Å (rotationally resolved IR spectroscopy at 50 K; Domenech *et al.*, 1994). ¶ R(O···O′) = 3.122 (1) and R(O···O″) = 3.098 (1) Å (neutron diffraction at 100 K; Kvick *et al.*, 1982).

Table 3
Atomic charges, Q, and electronic energies, E_{atom}, as well as the electronic energies per molecule, E_{mol}, computed by different methods.

Atomic experimental values are given in the first line, and theoretical values obtained from the B3LYP/cc-pVDZ/CRYSTAL (calculation 1) are listed in the second line.

Q_{atom} (e)	$-E_{atom}$ (hartree)		A	B	C	D
N 0.72	54.109	E_{mol} (hartree)	−409.290	−410.038	−410.038	−410.043
0.82	54.293					
O −0.36	75.268					
−0.41	75.363					

A: experiment, E_{mol} is the sum of E_{atom} values derived using the program *WinXPRO* (Stash & Tsirelson, 2002, 2005). B: direct calculation from the crystal wavefunction. C: E_{mol} is the sum of E_{atom} values derived using the program *TOPOND* (Gatti, 1999) from the crystal wavefunction. D: direct calculation from the single-molecule wavefunction (B3LYP/cc-pvDZ).

Laplacian distribution in the bond regions (Fig. 4). A similar observation has been previously reported for N—O and C—O bonds (Flaig *et al.*, 1998; Wagner & Luger, 2001; Tsirelson *et al.*, 2006; Zhurova, Stash *et al.*, 2006; Zhurova, Matta *et al.*, 2006). The disagreement is a consequence of insufficient flexibility of the Hansen–Coppens multipole model in

describing the covalent bonds formed by atoms with more than half-filled valence electron subshells (Tsirelson *et al.*, 2006, 2007; Volkov *et al.*, 2000; Dominiak & Coppens, 2006). At the same time, the theoretical ED presented in terms of the Hansen–Coppens multipole model yields BCP parameters which are very close to the experimental ones (see line 2 of Table 2).

The Cioslowski–Mixon (Cioslowski *et al.*, 1991) bond order of the N—N bond estimated for a single N_2O_4 molecule (wavefunction B3LYP/cc-pVDZ) is 0.51. The topological N—N bond-order index computed from experimental ED according to Tsirelson *et al.* (2007) is 0.42.[2] These values reflect the rather weak character of the N—N bond, which Messerschmidt *et al.* (2002) ascribed to the strong repulsion between the oxygen lone pairs and the positively charged N atoms. At first glance, the values of the atomic charges (Table 3) and the Laplacian distribution along the N—N line (Fig. 4) support this argument. However, the basins of the O atoms are well separated in the ESP gradient field by the basins of the N atoms (Fig. 2b) and there can therefore be no direct intramolecular O···O electrostatic repulsion forces in α-N_2O_4.

4.2. Intermolecular interactions: electron-density analysis

The previous theoretical QTAIMC studies (Bone & Bader, 1996; Bader, 1998; Hernández-Trujillo & Bader, 2000; Bader *et al.*, 2007) have shown that the mechanics of intermolecular bonding in van der Waals molecular systems is the same as that of closed-shell intramolecular bonding when viewed in terms of the Feynman, Ehrenfest and virial theorems. Indeed, both theory and experiment show (Tsirelson *et al.*, 1995; Boese *et al.*, 1997, 1999; Scherer *et al.*, 2000) that QTAIMC provides a set of intermolecular bond paths which detect and quantify van der Waals interactions. In α-N_2O_4 there are two symmetry-independent intermolecular O···O bond paths (marked as I and II), which differ by mutual orientations of the linked molecules (Fig. 1). They correspond to internuclear O···O distances of 3.116 (for I) and 3.094 Å (for II). Bond path I is practically a straight line, while bond path II is distinctly curved. The ellipticities, ε = 0.218 (I) and 0.436 (II), differ significantly reflecting the more prominent anisotropy of

[2] This quantity approximates the Cioslowski–Mixon (Cioslowski *et al.*, 1991) bond-order index.

Table 4
The results of the total N_2O_4 crystal structure optimization using different DFT methods (*CRYSTAL*06).

Here a is the unit-cell parameter, E is the electronic energy per primitive cell. The experimental value of a is 7.7529 (1) Å.

Approximation	a (Å)	E (a.u.)
BLYP/6-31G	8.012	−1230.49513
PBE/6-31G	7.858	−1229.46288
PWGGA/6-31G	7.880	−1230.34937
B3LYP/6-31G	7.849	−1229.98658
B3LYP/6-311G	7.957	−1230.36136
B3LYP/cc-pVDZ	7.780	−1230.13911
PBE/cc-pVDZ	7.802	−1229.61070
PBE/4-31G	7.778	−1227.73362
B3LYP/4-31G	7.742	−1228.23249
B3LYP/cc-pVDZ	7.774	−1230.13849
PBE/cc-pVDZ	7.798	−1229.61104
PWGGA/cc-pVDZ	7.823	−1230.50112

the electron density along the intermolecular contact II. The remaining BCP numerical characteristics of these bonds are practically the same (Table 2).

Tsirelson *et al.* (1998) and Dunitz & Gavezzotti (2005) pointed out that for interatomic and intermolecular regions in crystals where the ED is low, the identification and description of the bond paths and corresponding bond-critical points may not be obvious. The electron density values at the intermolecular BCPs in α-N_2O_4 are statistically significant, at least within 2 s.u.s (Table 2). To obtain additional evidence of whether or not the intermolecular BCPs in α-N_2O_4 reflect the molecular interactions, we searched for the same BCPs in the N_2O_4 procrystal – a hypothetical system consisting of spherical atoms placed in the positions occupied by real atoms in the crystal structure (Hirshfeld, 1971). Bond path I does not exist in the procrystal at all. However, it was found that 'quasi-BCPs' corresponding to bond paths II are located in the α-N_2O_4 procrystal. Although their characteristics differ only slightly from those of the BCP in a real crystal (see Table 2), the ED at the intermolecular BCP in a real crystal is lower; it is also shifted from the BCP towards the atomic cores. This behaviour is usually related to the effects of electron correlation, which diminishes the ED around the BCP (Gatti *et al.*, 1988; Boyd & Wang, 1988). Thus, the intermolecular 'BCPs' in a procrystal just result from the close proximity of molecules in a crystal and their specific arrangement, while both the intermolecular bond paths I and II do reflect molecular interactions in a crystalline α-N_2O_4.

To shed light upon the intermolecular interactions in crystalline α-N_2O_4, we note that the molecular recognition may be described in terms of molecular complementarity. In molecular systems without intermolecular hydrogen bonds, it is possible to distinguish two limiting complementarity mechanisms (Bader *et al.*, 1992; Matta & Bader, 2003). The van der Waals complementarity is determined by the size and shape of contacting atoms or atomic groups. In this case molecular interactions are proportional to the area of contact between the molecules, a quantity which can be measured by analyzing the intermolecular surfaces in terms of the QTAIMC model (Bader, 1990). In Lewis's complementarity

electrophilic (acidic) sites on one molecule fit into nucleophilic (basic) sites in another. QTAIMC allows the location of these sites by analyzing the Laplacian of the electron density $\nabla^2 \rho(\mathbf{r})$ (Bader *et al.*, 1984; Tsirelson *et al.*, 1995). The loss of spherical symmetry by the outer (valence) shells of bonded atoms leads to the formation of local electronic charge concentrations, forming local maxima of the $L(\mathbf{r}) = -\nabla^2\rho(\mathbf{r})$ function. The number, relative size and orientation of these local maxima correspond with the localized bonded and non-bonded Lewis electron pairs in the VSEPR model of molecular geometry (Gillespie, 1972). As the integral of $L(\mathbf{r})$ over an atomic basin vanishes, the appearance of regions with $L(\mathbf{r})>0$ ('lumps') is accompanied by the creation of regions with $L(\mathbf{r})<0$. The lumps show the presence of nucleophilic sites, while the local minima in $L(\mathbf{r})$ ('holes') denote regions of local depletions in electronic charge, locating the electrophilic activity sites. The complementary matching of lumps and holes in adjacent molecules influences the observed three-dimensional architecture of many molecular crystals (Tsirelson *et al.*, 1995; Boese *et al.*, 1997; Scherer *et al.*, 2000; Nelyubina *et al.*, 2007), as was predicted a long time ago by Kitaigorodsky (1973). Of course, in real systems, both van der Waals and Lewis complementarity mechanisms can occur simultaneously.

To establish which type of molecular complementarity dominates in α-N_2O_4, we computed the three-dimensional distribution of the Laplacian of the experimental electron density around the O atoms and superimposed it on the bond-path pattern (Fig. 6). We found that the maxima of local electron-density concentrations in the O-atom valence shells (*i.e.* the lumps in the negative Laplacian distribution) fit the holes on the O atoms in the adjacent molecules. In addition, the intermolecular bond path linking these atoms passes through the lumps and holes. Thus, we can say that Lewis-type complementarity significantly influences the observed three-dimensional structure in α-N_2O_4.

4.3. Intra- and intermolecular interactions: electrostatic potential analysis

We now consider the features of the electrostatic interactions in α-N_2O_4 in terms of the electrostatic potential (ESP), $\varphi(\mathbf{r})$, derived from the experimental electron density plus the nuclear contribution. The description of the main properties of the electrostatic (Coulomb) inner crystal field is available in the supplementary materials. We note here that the gradient lines of $\varphi(\mathbf{r})$ define the classic electrostatic field $\mathbf{E}(\mathbf{r}) = -\nabla\varphi(\mathbf{r})$ as well as the classic inner-crystal electrostatic force acting on the charge q at $\mathbf{r}$: $\mathbf{F}(\mathbf{r}) = q\mathbf{E}(\mathbf{r})$. The electric field $\mathbf{E}(\mathbf{r})$ and electric-field force $\mathbf{F}(\mathbf{r})$ vanish at the critical points in the ESP.

Gradient lines do not cross each other. Nuclei of neighbouring atoms in any crystal (as in a molecule) are separated in the electric field $\mathbf{E}(\mathbf{r})$ and electrostatic force field $\mathbf{F}(\mathbf{r})$ by surfaces P_i, satisfying the zero-flux condition

$$\mathbf{E}(\mathbf{r}) \cdot \mathbf{n}(\mathbf{r}) = -\nabla\varphi(\mathbf{r}) \cdot \mathbf{n}(\mathbf{r}) = \mathbf{F}(\mathbf{r}) \cdot \mathbf{n}(\mathbf{r}) = 0, \forall \mathbf{r} \in P_i(\mathbf{r}),$$

where $\mathbf{n}(\mathbf{r})$ is a unit vector normal to the surface P_i at $\mathbf{r}$. Each surface P_i defines the φ basin of the ith atom, inside of which

the nuclear charge Z_i is completely screened by the electronic charge, *i.e.* it defines the *electrically neutral bonded* pseudo-atom (Tsirelson *et al.*, 2001). In other words, surfaces P_i define the regions in a crystal dominated by a charge of a given nucleus: electron density within each φ basin is attracted to the corresponding nucleus.

The ESP distribution in α-N_2O_4 exhibits the well localized φ basins produced by the negatively charged O atoms. For the most part, they are immersed in the 'sea' of the ESP created by positively charged N atoms, being in some places in contact (see Fig. 2). No gradient lines connecting O atoms were found in the $\nabla\varphi(\mathbf{r})$ field; we have previously noted a similar observation for negatively charged atoms in other systems (Tsirelson *et al.*, 2000; Zhurova & Tsirelson, 2002).

Since electron density at the point $\mathbf{r}$ within a φ-basin around nucleus A is attracted to only nucleus A, it is useful to consider the superposition of the gradient fields (Fig. 3) to reconstruct the picture of the electrostatic forces acting in a crystal. If part of the electron density of atom A falls into the φ basin of the neighbouring atom B, the electron density of atom A is attracted to nucleus B. The combination of the $\nabla\rho(\mathbf{r})$ and $\nabla\varphi(\mathbf{r})$ gradient fields thus shows explicitly the picture of the interatomic and intermolecular electrostatic interactions in a molecule or a crystal. In α-N_2O_4, the ρ basins of the N atoms partially overlap the φ basins of adjacent O atoms both within each molecule and between the neighbouring molecules. The same picture is observed for ρ basins and φ basins of O atoms of neighbouring molecules (Fig. 3), reflecting the net electrostatic intermolecular attraction of the O atoms. This occurs even though they carry the same charges.

In general, the overlap of adjacent atomic ρ basins and φ basins is not necessarily accompanied by the formation of bond paths in the electron density between corresponding atoms. This implies that the electrostatic interaction picture does not exhibit directional character commonly associated with the bond paths. At the same time, consideration of the ESP distribution in the crystalline α-N_2O_4 mapped onto the 0.05 e Å^{-3} isodensity surface enables the correspondence between the ESP values along the bond paths to be visualized (Fig. 7). Indeed, the bond paths I and II run through the slightly differing ESP values on the 0.05 e Å^{-3} electron-density surfaces close to the BCP between adjacent molecules. In the other words, a potential difference occurs along the bond paths. Thus, the Lewis complementary matching of molecules is observed in terms of the ESP as well as in the Laplacian analysis described in §4.2.

Superposition of the $\nabla\rho(\mathbf{r})$ and $\nabla\varphi(\mathbf{r})$ gradient fields (Fig. 3a) allows better understanding of the nature of the rather long N—N bond. Messerschmidt *et al.* (2002) have attributed this to the strong repulsion between the oxygen lone pairs and the positively charged N atoms. However, the picture of the gradient fields does not support this: the basins of the O atoms are well separated in the ESP gradient field by the basins of the N atoms (Fig. 2b) showing that direct intramolecular O···O electrostatic repulsion forces do not exist in α-N_2O_4. Moreover, no overlap of the ρ basin and φ basin of the N atoms forming the N—N bond is observed. Thus, the N—N interaction is realised by means of interference, exchange and correlation electronic effects, which are relatively weak.

4.4. Exchange and correlation energy-density analysis

The exchange-correlation energy describes a contribution of non-classical electron–electron interactions to the total energy resulting from the same spin and spin-independent correlation in the electron motion. In DFT this energy is decomposed into the exchange and correlation parts which are often expressed by means of the functionals, including the exchange energy density per electron, $e_x(\mathbf{r})$, and the correlation energy density per electron, $e_c(\mathbf{r})$ (Parr & Yang, 1989; Dreizler & Gross, 1990). Functions $e_x(\mathbf{r})$ and $e_c(\mathbf{r})$ are not uniquely defined: they can be altered by the addition of any functional of electron density that integrates to zero over the density, or by a coordinate transformation (Baerends & Gritsenko, 1997; Springborg, 1990; Tao *et al.*, 2003). Despite this, in DFT these density functions carry important information, explicitly revealing the regions of potential energy lowering in molecules and crystals caused by electron exchange and correlation. This means that the exchange and correlation energy
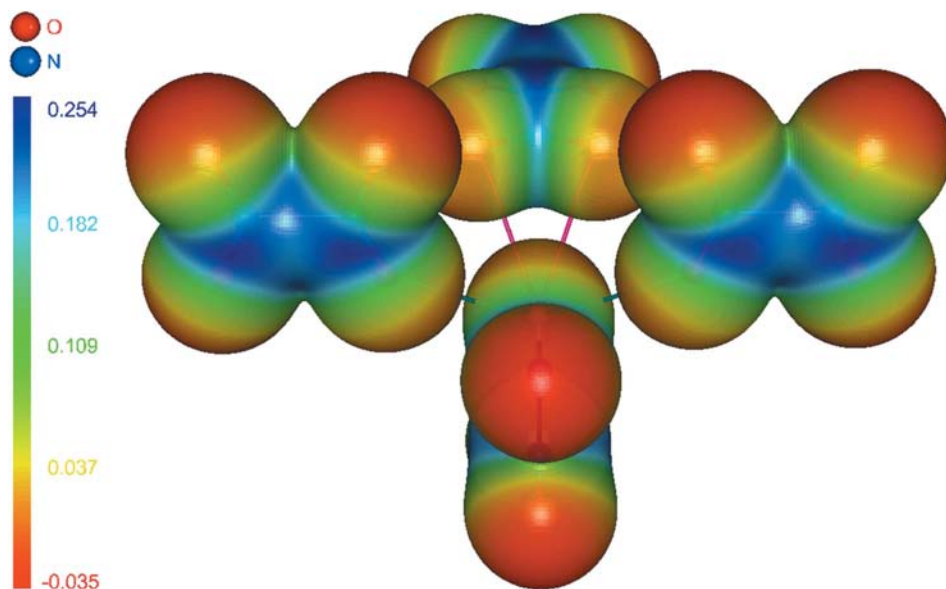

Figure 7
Three-dimensional isosurfaces of the experimental electrostatic potential in the N_2O_4 crystal projected into the three-dimensional isosurfaces of experimental electron density of 0.05 e Å^{-3} and superimposed on the O···O intermolecular bond paths of type I (pink) and type II (green).

functions may be used to detect the features of intermolecular interactions in α-N_2O_4.

There are a few DFT approximations which allow expression of $e_x(\mathbf{r})$ and $e_c(\mathbf{r})$ via $\rho(\mathbf{r})$, $\nabla\rho(\mathbf{r})$ and $\nabla^2\rho(\mathbf{r})$ (see reviews in Perdew & Kurth, 2003; von Barth, 2004; Scuseria & Staroverov, 2005). Following Tsirelson & Stash (2004) and Tsirelson (2007), we computed functions $e_x(\mathbf{r})$ and $e_c(\mathbf{r})$ using the experimental electron density and its derivatives. The Becke (1988b) approximation was used for $e_x(\mathbf{r})$ and Lee et al. (1991) formula was employed for $e_c(\mathbf{r})$. These local energies are presented in Fig. 8.

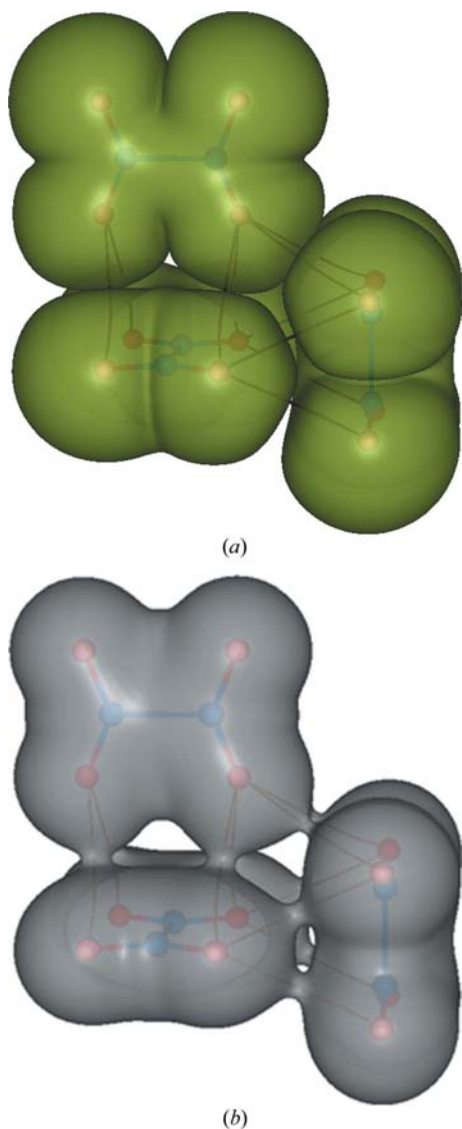The maps of e_x (Fig. 8a) show that exchange energy is concentrated in the atomic basins. Negative exchange energy-density bridges are not found between molecules, indicating that electron exchange does not contribute explicitly to the intermolecular interactions in α-N_2O_4 along the bond paths. By contrast, the three-dimensional image of function e_c (Fig. 8b) shows that the correlation energy contribution in the intermolecular region decreases the local potential energy along the intermolecular electron-density bond paths I and II. This is completely consistent with Feynman's (1939) statement that van der Waals interactions lead to electron-density concentration between linked atoms. It also establishes that the correlation energy density approximated by the Lee–Yang–Parr gradient-corrected functional (Lee et al., 1991) is able to describe the intermolecular bonding 'bridges' decreasing the local electronic energy along the $O\cdots O$ bond paths. This finding justifies our usage of the 'parent' LYP functional (Lee et al., 1988) in theoretical calculations.

5. Concluding remarks

We have studied the atomic and molecular interactions in a crystal of dinitrogen tetroxide, α-N_2O_4 in terms of the QTAIMC using high-resolution low-temperature X-ray diffraction data and CRYSTAL/DFT B3LYP/cc-pVDZ calculations. It was found that the crystalline α-N_2O_4 shows two types of intermolecular bond paths between O atoms, one measuring 3.116 Å (I) and another of 3.094 Å (II). Distribution of the Laplacian of electron density around the O atoms showed that the lumps in the negative Laplacian fit the holes on the O atoms in the adjusted molecules, both atoms are linked by the intermolecular bond paths. This was interpreted in terms of the fit between local concentrations and depletions of the electron density in neighbouring molecules. This leads to a Lewis-type molecular complementarity in the intermolecular interactions that direct the arrangement of molecules in the α-N_2O_4 crystal structure.

The superposition of the gradient fields in electron density and electrostatic potential revealed that nondirectional electrostatic atomic and molecular interactions in α-N_2O_4 crystals are realised as a consequence of the partial overlap of neighbouring atomic basins in the electron density and zero-flux basins in the electrostatic potential. The physical mechanism of the electrostatic interactions is the same both for intramolecular shared-shell interactions and intermolecular van der Waals closed-shell interactions. In particular, it clarifies why the electrostatic interaction of the same-sign charged O atoms in dinitrogen tetraoxide is attractive and contributes to forming the bonding $O\cdots O$ interaction. The bond paths I and II run through the electrostatic potential difference in the region around intermolecular BCPs between the adjacent molecules. Thus, the complementary matching of molecules is also observed in terms of the electrostatic potential.

Consideration of the exchange and correlation energy densities computed using the model functional and experimental electron density and its derivatives enabled the detection of features of the intermolecular interactions in α-N_2O_4. It was found that the intermolecular interactions in α-

Figure 8
(a) Three-dimensional isosurface of the Becke (1988) exchange energy density per electron, $\varepsilon_x(\mathbf{r}) = -0.15$ hartree/electron and (b) three-dimensional isosurface of the Lee–Yang–Parr gradient-corrected correlation energy density per electron $\varepsilon_c(\mathbf{r}) = -0.2 \times 10^{-3}$ hartree/electron derived from the experimental electron density. The latter figure shows the intermolecular 'bridges' along the $O\cdots O$ bond paths decreasing the local electronic energy.

N_2O_4 are accompanied by the correlation energy density 'bridges' lowering the local potential energy along the intermolecular $O \cdots O$ bond paths in the electron density, while the exchange energy density governs the shape of bounded molecules.

The correlation and exchange energy densities naturally extend a set of the real-space functions which are considered in QTAIMC. Analysis of these functions together with electron density and electrostatic potential provides insight into the bonding and binding in solids. In particular, it reveals the nature of the interactions which hold together the α-N_2O_4 molecules in a crystal.

References

Abrahams, S. C. & Keve, E. T. (1971). *Acta Cryst.* A**27**, 157–165.
Anantharaj, V., Bhonsle, J., Canteenwala, T. & Chiang, L. Y. (1999). *J. Chem. Soc. Perkin Trans. 1*, pp. 31–36.
Andersson, K. & Roos, B. (1993). *Int. J. Quantum Chem.* **45**, 591–607.
Angew, S. F., Swanson, B. I., Jones, L. H., Mills, R. L. & Schiferl, D. (1983). *J. Phys. Chem.* **87**, 5065–5068.
Bader, R. F. W. (1990). *Atoms in Molecules: A Quantum Theory*, pp. 1–438. Oxford: Clarendon Press.
Bader, R. F. W. (1998). *J. Phys. Chem. A*, **102**, 7314–7323.
Bader, R. F. W. & Beddall, P. M. (1972). *J. Chem. Phys.* **56**, 3320–3329.
Bader, R. F. W., Hernández-Trujillo, J. & Cortés-Guzmán, F. (2007). *J. Comput. Chem.* **28**, 4–14.
Bader, R. F. W., MacDougall, P. J. & Lau, C. D. H. (1984). *J. Am. Chem. Soc.* **106**, 1594–1605.
Bader, R. F. W., Popelier, P. L. A. & Chang, C. J. (1992). *J. Mol. Struct. THEOCHEM*, **255**, 145–171.
Baerends, E. J. & Gritsenko, O. V. (1997). *J. Phys. Chem. A*, **101**, 5383–5403.
Balanarayan, P. & Gadre, S. R. (2003). *J. Chem. Phys.* **119**, 5037–5043.
Barth, U. von (2004). *Phys. Scr.* **T109**, 9–39.
Bauschlicher, C. W., Komornicki, A. & Roos, B. (1983). *J. Am. Chem. Soc.* **105**, 745–748.
Becke, A. D. (1988*a*). *J. Chem. Phys.* **88**, 2547–2553.
Becke, A. D. (1988*b*). *Phys. Rev. A*, **38**, 3098–3100.
Becke, A. D. (1993). *J. Chem. Phys.* **98**, 5648–5652.
Becker, P. J. & Coppens, P. (1974). *Acta Cryst.* A**30**, 129–147.
Betteridge, P. W., Carruthers, J. R., Cooper, R. I., Prout, K. & Watkin, D. J. (2003). *J. Appl. Cryst.* **36**, 1487.
Blessing, R. H. (1987). *Cryst. Rev.* **1**, 3–58.
Blessing, R. H. (1989). *J. Appl. Cryst.* **22**, 396–397.
Boese, R., Blaser, D., Heinemann, O., Abramov, Yu., Tsirelson, V. G., Blaha, P. & Schwarz, K. (1999). *J. Phys. Chem. A*, **103**, 6209–6213.
Boese, R., Boese, A. D., Blaser, D., Antipin, M. Yu., Ellern, A. & Seppelt, K. (1997). *Angew. Chem. Int. Ed. Engl.* **36**, 1489–1492.
Boese, R. & Nussbaumer, M. (1994). *Correlations, Transformations, and Interactions in Organic Crystal Chemistry*, edited by D. W. Jones & A. Katrusiak, Vol. 7, IUCr Crystallographic Symposia, pp. 20–37. Oxford University Press.
Bolduan, F. & Jodl, H. J. (1982). *J. Chem. Phys. Lett.* **85**, 283–286.
Bolduan, F., Jodi, H. J. & Loewenschuss, A. (1984). *J. Chem. Phys.* **80**, 1739–1743.
Bone, R. G. A. & Bader, R. F. W. (1996). *J. Phys. Chem. B*, **100**, 10892–10911.
Bouhmaida, N., Dutheil, M., Ghermani, N. E. & Becker, P. J. (2002). *Chem. Phys.* **116**, 6196–6204.
Boyd, R. J. & Wang, L. C. (1988). *J. Comput. Chem.* **10**, 367–375.
Boyer, J. H. & Pillai, T. P. (1985). *J. Chem. Soc. Perkin Trans. 1*, pp. 1661–1664.
Chałasiński, G. & Szczęśniak, M. (1994). *Chem. Rev.* **94**, 1723–1765.
Cioslowski, J., Mixon, S. T. & Fleischmann, E. D. (1991). *J. Am. Chem. Soc.* **113**, 4751–4755.
Chesnut, D. B. & Crumbliss, A. L. (2005). *Chem. Phys.* **315**, 53–58.
Domenech, J. L., Andrews, A. M., Belov, S. P., Fraser, G. T. & Lafferty, W. J. (1994). *J. Chem. Phys.* **100**, 6993–6999.
Dominiak, P. M. & Coppens, P. (2006). *Acta Cryst.* A**62**, 224–227.
Dovesi, R., Saunders, V. R., Roetti, C., Orlando, R., Zicovich-Wilson, C. M., Pascale, F., Civalleri, B., Doll, K., Harrison, N. M., Bush, I. J., D'Arco, P. & Llunell, M. (2006). *CRYSTAL06 User's Manual.* Universita' di Torino, Italy.
Dreizler, R. M. & Gross, E. K. U. (1990). *Density Functional Theory.* Berlin: Springer-Verlag.
Dunitz, J. D. & Gavezzotti, A. (2005). *Angew. Chem.* **44**, 1766–1787.
Dunning, T. H. Jr & Woon, D. E. (1995). *J. Chem. Phys.* **103**, 4572–4585.
Feynman, R. P. (1939). *Phys. Rev.* **56**, 340–343.
Flaig, R., Koritsanszky, T., Zobel, D. & Luger, P. (1998). *J. Am. Chem. Soc.* **120**, 2227–2238.
Gadre, S. R., Bhadane, P. K., Pundlik, S. S. & Pingale, S. S. (1996). *In Molecular Electrostatic Potentials: Concepts and Applications*, edited by J. S. Murray & K. D. Sen, p. 219. Amsterdam: Elsevier.
Gatti, C. (1999). *TOPOND*98. CNR-ISTM, Milan, Italy.
Gatti, C., MacDougall, P. J. & Bader, R. F. W. (1988). *J. Chem. Phys.* **88**, 3792–3804.
Giamalva, D. H., Kenion, G. B., Church, D. F. & Pryor, W. A. (1987). *J. Am. Chem. Soc.* **109**, 7059–7063.
Giauque, W. F. & Kemp, J. D. (1938). *J. Chem. Phys.* **6**, 40–52.
Gillespie, R. J. (1972). *Molecular Geometry*, pp. 1–226. London: Van Nostrand Reinhold.
Glendening, E. D. & Halpern, A. M. (2007). *J. Chem. Phys.* **127**, 164307.
Hansen, N. K. & Coppens, P. (1978). *Acta Cryst.* A**34**, 909–921.
Hernández-Trujillo, J. & Bader, R. F. W. (2000). *J. Phys. Chem. A*, **104**, 1779–1794.
Hisatsune, I. C., Devlin, J. P. & Wada, Y. (1960). *J. Chem. Phys.* **33**, 714–719.
Hirshfeld, F. L. (1971). *Acta Cryst.* B**27**, 769–781.
Hirshfeld, F. L. (1976). *Acta Cryst.* A**32**, 239–244.
Jones, L. H., Swanson, B. I. & Agnew, S. F. (1985). *J. Chem. Phys.* **82**, 4389–4390.
Kirzhnits, D. A. (1957). *Sov. Phys. JETP*, **5**, 64–72.
Kitaigorodsky, A. I. (1973). *Molecular Crystals and Molecules.* New York: Academic Press.
Koput, J. (1995). *Chem. Phys. Lett.* **240**, 553–559.
Kvick, A., McMullan, R. R. & Newton, M. D. (1982). *J. Chem. Phys.* **76**, 3754–3761.
Leboeuf, M., Köster, A. M., Jug, K. & Salahub, D. R. (1999). *J. Chem. Phys.* **111**, 4893–4905.
Leboeuf, M., Köster, A. M. & Salahub, D. R. (1997). *Theor. Chem. Acc.* **96**, 23–30.
Lee, C., Yang, W. & Parr, R. G. (1988). *Phys. Rev. B*, **37**, 785–789.
Lee, C., Yang, W. & Parr, R. G. (1991). *Phys. Rev. A*, **44**, 768–771.
Lobanov, N. N., Shchedrin, B. M. & Tsirelson, V. G. (1990). *Sov. Phys. Crystallogr.* **35**, 344–347.
Macchi, P. & Coppens, P. (2001). *Acta Cryst.* A**57**, 656–662.
Mata, I., Molins, E. & Espinosa, E. (2007). *J. Phys. Chem. A*, **111**, 9859–9870.
Matta, C. F. & Bader, R. F. W. (2003). *Proteins*, **52**, 360–399.
McClelland, B. W., Gundersen, G. & Hedberg, K. (1972). *J. Chem. Phys.* **56**, 4541–4545.
Mehta, G. & Uma, R. (1996). *Tetrahedron Lett.* **37**, 1897–1898.

Messerschmidt, M., Wagner, A., Wong, M. W. & Luger, P. (2002). *J. Am. Chem. Soc.* **124**, 732–733.

Miehlich, B., Savin, A., Stoll, H. & Preuss, H. (1989). *Chem. Phys. Lett.* **157**, 200–206.

Nelyubina, Yu. V., Antipin, M. Yu. & Lyssenko, K. A. (2007). *J. Phys. Chem. A*, **111**, 1091–1095.

Novakovic, S. B., Bogdanovic, G. A., Fraisse, B., Ghermani, N. E., Bouhmaida, N. & de Spasojevic, B. A. (2007). *J. Phys. Chem. A*, **111**, 13492–13505.

Oae, S., Shinhama, K. & Kim, Y. H. (1977). *J. Chem. Soc. Chem. Commun.* **12**, 407–408.

Oae, S., Shinhama, K. & Kim, Y. H. (1979). *Tetrahedron Lett.* **20**, 3307–3308.

Parr, R. G. & Yang, W. (1989). *Density-Functional Theory of Atoms and Molecules.* New York: Oxford University Press.

Parts, L. & Miller Jr, J. T. (1965). *J. Chem. Phys.* **43**, 136–139.

Pascale, F., Zicovich-Wilson, C. M., Gejo, F. L., Civalleri, B., Orlando, R. & Dovesi, R. (2004). *J. Comput. Chem.* **25**, 888–897.

Pathak, R. K. & Gadre, S. R. (1990). *J. Chem. Phys.* **93**, 1770–1773.

Perdew, J. P. (1991). *Electronic Structure of Solids*, edited by P. Ziesche & H. Eschrig, p. 11. Berlin: Akademie Verlag.

Perdew, J. P., Burke, K. & Ernzerhof, M. (1996). *Phys. Rev. Lett.* **77**, 3865–3868.

Perdew, J. P. & Kurth, S. (2003). *Lecture Notes in Physics*, edited by C. Fiolhais, F. Nogueira & M. Marques, pp. 1–55. Berlin: Springer-Verlag.

Politzer, P. & Parr, R. G. (1974). *J. Chem. Phys.* **61**, 4258–4262.

Protas, J. (1997). *MOLDOS*97/*MOLLY* IBM PC-DOS. Personal communication.

Reznik, I. M. (1992). *Electron Density Theory of Ground State Properties of Crystals.* Kiev: Naukova Dumka.

Scherer, W., Spiegler, M., Pedersen, B., Tafipolsky, M., Hieringer, W., Reinhard, B., Downs, A. J. & McGrady, G. S. (2000). *Chem. Commun.* **7**, 635–636.

Schlegel, H. B. (1982). *J. Comput. Chem.* **3**, 214–218.

Scuseria, G. E. & Staroverov, V. N. (2005). *Theory and Application of Computational Chemistry.* Amsterdam: Elsevier.

Sheldrick, G. M. (2008). *Acta Cryst.* A**64**, 112–122.

Siemens (1996). *SAINT.* Siemens X-ray Instruments Inc., Madison, Wisconsin, USA.

Springborg, M. (1990). *Chem. Phys. Lett.* **308**, 83–91.

Squadrito, G. L., Fronczek, F. R., Watkins, S. F., Church, D. F. & Pryor, W. A. (1990). *J. Org. Chem.* **55**, 4322–4326.

Stash, A. & Tsirelson, V. (2002). *J. Appl. Cryst.* **35**, 371–373.

Stash, A. I. & Tsirelson, V. G. (2005). *Crystallogr. Rep.* **50**, 202–209.

Tal, Y. & Bader, R. F. W. (1978). *Int. J. Quant. Chem. Symp.* **12**, 153–168.

Tao, J., Springborg, M. & Perdew, J. P. (2003). *J. Chem. Phys.* **119**, 6457–6464.

Tsirelson, V. G. (2007). *The Quantum Theory of Atoms in Molecules: From Solid State to DNA and Drug Design*, edited by C. Matta & R. Boyd, ch. 10, pp. 259–283. New York: Wiley-VCH.

Tsirelson, V., Abramov, Y., Zavodnik, V., Stash, A., Belokoneva, E., Stahn, J., Pietsch, U. & Feil, D. (1998). *Struct. Chem.* **9**, 249–254.

Tsirelson, V. G., Avilov, A. S., Lepeshov, G. G., Kulygin, A. K., Stahn, J., Pietsch, U. & Spence, J. C. H. (2001). *J. Phys. Chem. B*, **105**, 5068–5074.

Tsirelson, V. G., Bartashevich, E. V., Stash, A. I. & Potemkin, V. A. (2007). *Acta Cryst.* B**63**, 142–150.

Tsirelson, V., Ivanov, Y., Zhurova, E., Zhurov, V. & Tanaka, K. (2000). *Acta Cryst.* B**56**, 197–203.

Tsirelson, V. G. & Ozerov, R. P. (1996). *Electron Density and Bonding in Crystals.* Bristol, Philadelphia: Institute of Physics Publishing.

Tsirelson, V. & Stash, A. (2004). *Acta Cryst.* A**60**, 418–426.

Tsirelson, V. G., Stash, A. I., Potemkin, V. A., Rykounov, A. A., Shutalev, A. D., Zhurova, E. A., Zhurov, V. V., Pinkerton, A. A., Gurskaya, G. V. & Zavodnik, V. E. (2006). *Acta Cryst.* B**62**, 676–688.

Tsirelson, V. G., Zhou, P. F., Tang, T.-H. & Bader, R. F. W. (1995). *Acta Cryst.* A**51**, 143–153.

Volkov, A., Abramov, Y., Coppens, P. & Gatti, C. (2000). *Acta Cryst.* A**56**, 332–339.

Wagner, A. & Luger, P. (2001). *J. Mol. Struct.* **595**, 39–46.

Wesolowski, S. S., Fermann, J. T., Crawford, T. D. & Schaefer, H. F. (1997). *J. Chem. Phys.* **106**, 7178–7184.

Zakharov, I. I., Kolbasin, A. I., Zakharova, O. I., Kravchenko, I. V. & Dyshlovoi, V. I. (2008). *Theor. Exp. Chem.* **44**, 26–31.

Zhurova, E. A., Matta, C. F., Wu, N., Zhurov, V. V. & Pinkerton, A. A. (2006). *J. Am. Chem. Soc.* **128**, 8849–8862.

Zhurova, E. A., Stash, A. I., Tsirelson, V. G., Zhurov, V. V., Bartashevich, E. V., Potemkin, V. A. & Pinkerton, A. A. (2006). *J. Am. Chem. Soc.* **128**, 14728–14734.

Zhurova, E. A. & Tsirelson, V. G. (2002). *Acta Cryst.* B**58**, 567–575.

Zhurova, E. A., Tsirelson, V. G., Stash, A. I. & Pinkerton, A. A. (2002). *J. Am. Chem. Soc.* **124**, 4574–4575.

Zhurova, E. A., Zuo, J. M. & Tsirelson, V. G. (2001). *J. Phys. Chem. Solids*, **62**, 2143–2146.